Inorg. Chem. **2004**, *43*, 4962–4973

Analysis of Low Oxidation State Transition Metal Clusters by Laser Desorption/Ionization Time-of-Flight Mass Spectrometry

Paul J. Dyson,*,† Andrew K. Hearley,‡ Brian F. G. Johnson,*,‡ Patrick R. R. Langridge-Smith,§ and J. Scott McIndoe*,||

Institut des Sciences et Ingénierie Chimiques, Ecole Polytechnique Fédérale de Lausanne, EPFL-BCH, CH-1015 Lausanne, Switzerland, Department of Chemistry, The University of Cambridge, Lensfield Road, Cambridge, CB2 1EW, U.K., Department of Chemistry, The University of Edinburgh, West Mains Road, Edinburgh, EH9 3JJ, U.K., and Department of Chemistry, The University of Victoria, P.O. Box 3065, Victoria, BC V8W 3V6, Canada

Received April 27, 2004

A variety of homonuclear and heteronuclear transition metal carbonyl clusters have been analyzed by ultraviolet laser desorption/ionization time-of-flight mass spectrometry. The spectra were recorded in negative and positive ion modes, using both linear and reflective techniques. A range of different clusters based on different nuclearities, geometries, and ligand types, which include hydrides, phosphines, nitriles, and cyclopentadienyl ligands and naked main group atoms, were studied. These experiments have allowed us to construct a detailed picture of the technique for the analysis of transition metal carbonyl clusters and their derivatives. In general, extensive reactions are observed, cluster aggregation reactions in particular, and from a comparison of the spectra obtained, some mechanistic inferences concerning the aggregation processes have been drawn.

Introduction

Mass spectrometry has been widely employed by cluster chemists to facilitate the characterization of novel compounds prepared in the laboratory.[1] Techniques such as electron impact ionization (EI)[2] and fast atom/ion bombardment (FAB/FIB)[3] have been routinely used for many years by cluster chemists. There are more techniques now available including plasma desorption, electrospray ionization (ESI), and matrix-assisted laser desorption/ionization (MALDI) mass spectrometry. Electrospray ionization mass spectrometry has been applied to the analysis of clusters with considerable success.[4] One of the key features is that, under the right conditions, peaks corresponding to intact clusters can be obtained without any fragmentation. A variant to ESI is energy-dependent electrospray ionization mass spectrometry,[5] which has been shown to resolve mixtures of clusters allowing the assignment of each component in the mixture.[6] In contrast, plasma desorption and MALDI mass spectrometry have been used considerably less for the analysis of carbonyl clusters,[7] despite the technique being ideally suited to solid substrates with low volatilities and high molecular weights.[8] Although plasma desorption has been largely superseded by MALDI, there is an interesting comparison in that both techniques result in the aggregation of clusters and the formation of what have been termed supraclusters (see text to follow).[9]

* Authors to whom correspondence should be addressed. E-mail: paul.dyson@epfl.ch (P.J.D.); bfgjl@cam.ac.uk (B.F.G.J.); mcindoe@uvic.ca (J.S.M.).

† Ecole Polytechnique Fédérale de Lausanne.

‡ The University of Cambridge.

§ The University of Edinburgh.

|| The University of Victoria.

(1) (a) Colton, R.; D'Agostino, A.; Traeger, J. C. *Mass Spectrom. Rev.* **1995**, *14*, 79. (b) Johnson, B. F. G.; McIndoe, J. S. *Coord. Chem. Rev.* **2000**, *200*, 901.

(2) (a) Litzow, M. R.; Spalding, T. R. *Mass Spectrometry of Inorganic and Organometallic Compounds*; Elsevier: Amsterdam, 1973. (b) Charalambous, J., Ed. *Mass Spectrometry of Metal Compounds*; Butterworth & Co: London 1975.

(3) Bruce, M. I.; Liddell, M. J. *Appl. Organomet. Chem.* **1987**, *1*, 191.

(4) (a) Henderson, W.; McIndoe, J. S.; Nicholson, B. K.; Dyson, P. J. *Chem. Commun.* **1996**, 1183. (b) Henderson, W.; McIndoe, J. S.; Nicholson, B. K.; Dyson, P. J. *J. Chem. Soc., Dalton Trans.* **1998**, 519.

(5) (a) Dyson, P. J.; Johnson, B. F. G.; McIndoe, J. S.; Langridge-Smith, R. R. *Rapid Commun. Mass Spectrom.* **2000**, *14*, 311. (b) Dyson, P. J.; Hearley, A. K.; Johnson, B. F. G.; McIndoe, J. S.; Langridge-Smith, P. R. R.; Whyte, C. *Rapid Commun. Mass Spectrom.* **2001**, *15*, 895. (c) Dyson, P. J.; Feeder, N.; Johnson, B. F. G.; McIndoe, J. S.; Langridge-Smith, P. R. R. *J. Chem. Soc., Dalton Trans.* **2000**, 1813.

(6) Dyson, P. J.; Hearley, A. K.; Johnson, B. F. G.; Khimyak, T.; McIndoe, J. S.; Langridge-Smith, P. R. R. *Organometallics* **2001**, *20*, 3970.

(7) McIndoe, J. S. *Transition Met. Chem.* (*Dordrecht, Neth.)* **2003**, *28*, 122.

(8) Fisher, K. J. *Prog. Inorg. Chem.* **2001**, *50*, 343.

10.1021/ic049458i CCC: $27.50 © 2004 American Chemical Society
Published on Web 07/03/2004

Transition metal carbonyl complexes are known to undergo ion−molecule clustering in the gas phase; this phenomenon has been observed using EI mass spectrometry [5] for simple complexes such as $Ni(CO)_4$, $Fe(CO)_5$, $Co(NO)(CO)_3$, and $Cr(CO)_6$.[10] The development of FTICR mass spectrometry enabled much more detailed studies of such gas-phase reactions because of the very high mass resolution of the technique and the ability to extend the time scale of the experiment. Clusters have been examined using EI-FTICR, with cluster cations as large as $[Mn_8(CO)_{25}]^+$ formed from $Mn_2(CO)_{10}$, and $[Re_3Mn_3(CO)_{19}]^+$ from $ReMn(CO)_{10}$.[11] In similar experiments on $Os_3H_2(CO)_{10}$, self-reaction via gas-phase ion−molecule reactions has been found to produce clusters containing up to 15 osmium atoms upon extended ($\geq$0.5 s) trapping.[12]

In this paper, we describe the results from a study in which a broad range of transition metal carbonyl cluster compounds were analyzed by LDI mass spectrometry (i.e., no matrix assistance), a technique that is now routinely available in many laboratories. We show the type of information that is obtained using this technique and indicate where caution must be applied when interpreting these types of spectra.

Results and Discussion

Anionic Clusters. The laser desorption/ionization time-of-flight (LDI-TOF) mass spectra of a broad range of cluster compounds have been recorded. The spectra of anionic clusters are relatively straightforward to assign, as noted previously,[13] whereas the spectra obtained for neutral compounds exhibit many complicated features that require detailed analysis and interpretation. The cluster anions $[Ru_3Co(CO)_{13}]^-$ **1**, $[Ru_3Ir(CO)_{13}]^-$ **2**, $[H_3Os_4(CO)_{12}]^-$ **3**, $[HRu_6(CO)_{18}]^-$ **4**, $[Ru_5CoC(CO)_{16}]^-$ **5**, $[Ru_5IrC(CO)_{16}]^-$ **6**, $[Fe_6C(CO)_{16}]^{2-}$ **7**, $[Ru_6C(CO)_{16}]^{2-}$ **8**, $[Re_8C(CO)_{24}]^{2-}$ **9**, $[HRu_{10}C(CO)_{24}]^-$ **10**, and $[Os_{10}C(CO)_{24}]^{2-}$ **11** have been analyzed using negative ion LDI−TOF mass spectrometry, and the results are summarized in Table 1. The effect of the matrix was explored, and it was found that, in keeping with other types of inorganic/organometallic compounds,[14] the best results were obtained in the absence of any matrix. As such, the cluster analyte is dissolved in a volatile solvent, typically dichloromethane, and deposited directly onto the sample probe. The solvent is allowed to evaporate, leaving a thin layer of the pure sample, and several layers are added in this manner.

Table 1: Peak Relative Intensities in the LDI Mass Spectra of Clusters **1**−**11**

	1	**2**	**3**	**4**	**5**	**6**	**7**	**8**	**9**	**10**	**11**
$[M]^-$	11		70		80	43	20	100	100	84	8
$[M-CO]^-$	54	4	100	3	100	100	100	80	14	100	9
$[M-2CO]^-$	100	50	35	54	70	92	83	31	41	63	13
$[M-3CO]^-$	35	100	5	54	36	43	11	10	9	59	18
$[M-4CO]^-$	22	58	6	25	14	22	10	9	53	57	22
$[M-5CO]^-$	9	8		10	7	7	3	8	25	46	31
$[M-6CO]^-$	3	3		100	2		2	7	68	42	68
$[M-7CO]^-$	3			41				6	2	21	100
$[M-8CO]^-$				10				5	1	13	87
$[M-9CO]^-$				9				4		9	72
$[M-10CO]^-$				7				3		6	67
$[M-11CO]^-$				4				2		4	50
$[M-12CO]^-$				13				2		2	36
$[M-13CO]^-$								2			24
$[M-14CO]^-$											18
$[M-15CO]^-$											13
$[M-16CO]^-$											7
$[M-17CO]^-$											3

In general, the spectra of **1**−**11** show similar features, and consequently, they may be discussed together. The parent ion for the cluster anions is generally observed together with the loss of a number of CO ligands. However, parent ions were not observed for **2** or **4** at the laser power employed, so caution must be applied when using LDI−MS to investigate cluster anions for the purpose of establishing the molecular ion. Figure 1 shows the LDI mass spectrum of **2**, clearly demonstrating the absence of the molecular ion.

One precaution that may be taken to improve the chances of establishing the molecular ion is to modulate the laser power such that the intensity of the laser is only just above the threshold for ion production (the exact threshold is dependent on the instrument used). Under such conditions, the intensities of the higher-mass ions (i.e., those that have lost none or only a few carbonyl ligands) are enhanced. As expected, increasing the laser power has a corresponding effect on the extent to which the carbonyl ligands are eliminated, and at high enough laser power, the bare metal core can even be generated.

All of the dianionic clusters analyzed, viz. **7**−**9** and **11**, are observed as monoanions, which could lead to confusion

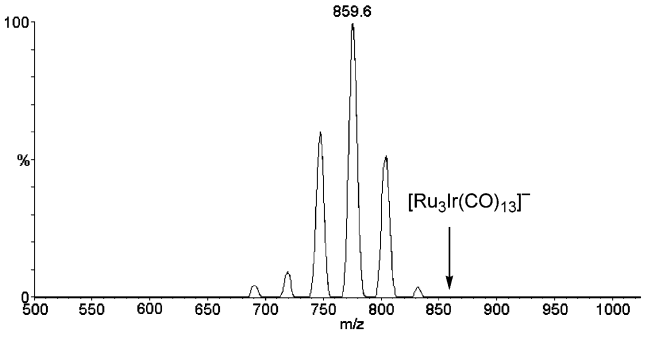

Figure 1. Negative ion mass spectra of $[Ru_3Ir(CO)_{13}]^-$ **2**. Note the absence of the molecular ion.

(9) (a) Fackler, J. P., Jr.; McNeal, C. J.; Winpenny, R. E. P. *J. Am. Chem. Soc.* **1989**, *111*, 6434. (b) Feld, H.; Leute, A.; Rading, D.; Benninghoven, A.; Schmid, G. *J. Am. Chem. Soc.* **1990**, *112*, 8166. (c) McNeal, C. J.; Hughes, J. M.; Lewis, G. J.; Dahl, L. F. *J. Am. Chem. Soc.* **1991**, *113*, 372. (d) McNeal, C. J.; Winpenny, R. E. P.; Hughes, J. M.; Macfarlane, R. D.; Pignolet, L. H.; Nelson, L. T. J.; Irgens, T. G.; Vigh, G.; Fackler J. P., Jr. *Inorg. Chem.* **1993**, *32*, 5582.

(10) (a) Allison, J.; Ridge, D. P. *J. Am. Chem. Soc.* **1979**, *101*, 4998. (b) Foster, M. S.; Beauchamp, J. L. *J. Am. Chem. Soc.* **1971**, *93*, 4924. (c) Foster, M. S.; Beauchamp, J. L. *J. Am. Chem. Soc.* **1975**, *97*, 4808. (d) Weddle, G. H.; Allison, J.; Ridge, D. P. *J. Am. Chem. Soc.* **1977**, *99*, 105. (e) Kraihanzel, C. S.; Conville, J. J.; Sturm, J. E. *J. Chem. Soc., Chem. Commun.* **1971**, 159.

(11) Meckstroth, W. K.; Freas, R. B.; Reents, W. D., Jr.; Ridge, D. P. *Inorg. Chem.* **1985**, *24*, 3139.

(12) Mullen, S. L.; Marshall A. G. *J. Am. Chem. Soc.* **1988**, *110*, 1766.

(13) (a) Dyson, P. J.; Hearley, A. K.; Johnson, B. F. G.; McIndoe, J. S.; Langridge-Smith, P. R. R. *J. Cluster Sci.* **2001**, *12*, 273. (b) Dyson, P. J.; Johnson, B. F. G.; McIndoe, J. S.; Langridge-Smith, P. R. R. *Inorg. Chem.* **2000**, *39*, 2430.

(14) (a) Stulz, E.; Mak, C. C.; Sanders, J. K. M. *J. Chem. Soc., Dalton Trans.* **2001**, 604. (b) Dorcier, A.; Dyson, P. J.; McIndoe, J. S. *Eur. J. Inorg. Chem.* **2003**, 4294. (c) Hearley, A. K.; Johnson, B. F. G.; McIndoe, J. S.; Tuck, D. G. *Inorg. Chim. Acta* **2002**, *334*, 105.

unless the masses of the clusters are assessed in combination with electron counting rules. For example, an octahedral cluster requires 86 cluster valance electrons (cve's), and $[Ru_6C(CO)_{16}]^-$ has only 85 cve's. Bearing in mind that multiple charges on clusters are always oxidized to monoanions by the LDI method, it is not unreasonable to assume that the actual structural formula is $[Ru_6C(CO)_{16}]^{2-}$. However, this simple manipulation becomes less certain as the cluster nuclearity increases, because the electron counting rules become less reliable.[15] Electrospray ionization mass spectrometry is very effective for the analysis of cluster anions without moderation of the charge.[16] As such, a di- or trianion is observed as an *m*/*z* multiply charged anion, and the isotope pattern allows the charge state to be easily determined. There is a caveat here, however: multiply charged anions have a limited existence in the gas phase,[17] and it is only those of high molecular weight that can carry multiple charges without undergoing an electron autodetachment event. Clusters have been observed to lose an electron at a specific point in the collision-induced dissociation (CID) fragmentation process, corresponding to the point at which the electron binding energy (determined by gas-phase photoelectron spectroscopy) drops to zero.[18]

Neutral Clusters. The LDI mass spectra of neutral clusters are considerably more complicated than those of their anionic counterparts. The absence of aggregation species in the LDI mass spectra of anionic clusters contrasts sharply with the situation for similar neutral clusters, the spectra of which are dominated by high-mass cluster aggregates. The reason for this absence in anionic clusters is almost certainly that the gas-phase reactivity of like-charged clusters is negligible because of charge repulsion. With neutral clusters, extensive reactions take place leading to the formation of what have been termed supraclusters, suggesting that gas-phase reactivity is represented by ion/neutral, positive-ion/negative-ion, or neutral/neutral reactions. The range of compounds studied shows that the supraclustering process critically depends upon the size and geometry of the cluster core. The natures of the ligands attached to the cluster also have an influence, but to a lesser extent. The spectra obtained in negative and positive ion mode are qualitatively similar. The only significant difference between the two modes is that, in negative ion mode, peaks extended to higher masses. The nature of the highest mass peak observed in the parent ion region also differs (see text to follow).

A detailed analysis of the LDI mass spectra of the trinuclear clusters $M_3(CO)_{12}$ (M = Fe **12**, Ru **13**, and Os **14**) has been reported previously,[19] from which the following general features emerged:

(i) In negative ion mode, peaks corresponding to the intact parent cluster ion are not observed; instead, the highest observed M_3 peak corresponds to $[M_3(CO)_{11}]^-$.

(ii) In positive ion mode, peaks corresponding to clusters in which an additional CO ligand is attached to the parent are observed (i.e., for $[M_3(CO)_{12}]$, the observed parent ion is $[M_3(CO)_{13}]^+$).

(iii) Peaks are observed at higher masses than that of the M_3 precursor, which correspond to the formation of higher nuclearity clusters with nuclearities of 4, 5, 6, and so forth. The least clustering was observed for $Os_3(CO)_{12}$, and the most was observed for $Fe_3(CO)_{12}$, presumably because of the differences in metal−metal bond strengths among these three transition metals.

(iv) Peaks arising from post-source decay (dissociation of the cluster aggregates outside of the ion extraction region) are observed. This process takes place only when the spectra are recorded in reflectron mode, and it has the effect of perturbing the centroid of the isotope envelopes for certain peaks, which complicates analysis.

The effect of the matrix on aggregation has also been explored. In general, diluting a neutral cluster in a matrix such as dithranol reduces the number of gas-phase reaction products that are observed in the spectrum. Other matrixes behave similarly and/or simply reduce the signal-to-noise ratio without significantly affecting the product ion distribution. As such, neutral clusters were analyzed in the absence of the matrix. Transition metal carbonyl clusters absorb strongly enough in the UV range to act as suitable matrixes themselves.

The negative ion LDI mass spectra of $Ru_6C(CO)_{17}$ **15**, $Ru_6C(CO)_{14}(\eta^6\text{-}C_6H_5Me)$ **16**, and $Ru_6C(CO)_{12}(\eta^6\text{-}C_6H_5Me)(\mu\text{-}C_6H_7Me)$ **17**,[20] $Rh_6(CO)_{16}$ **18**,[21] and $Os_6(CO)_{18}$ **19**[22] have been previously published and provided useful mechanistic insights into the supraclustering process. In each case, the main feature was the formation of supraclusters, aggregates of the clusters in multiples of the original nuclearity of six, to give clusters of the general formula $[(M_6)_n(CO)_m]^{+/-}$. Supraclustering of **18** extended well beyond 5000 *m*/*z*, representing $[Rh_{42}(CO)_x]^-$ and $[Rh_{48}(CO)_x]^-$ clusters (Figure 2).

The aggregate peaks present in the spectrum shown in Figure 2 are typical of both negative and positive ion spectra, although in general, negative ions give rise to aggregation products extending to higher masses and with higher intensities than the positive ions. From a synthetic viewpoint, large clusters tend to be anionic,[23] and therefore, it is not unreasonable that higher nuclearity clusters are observed by LDI-MS when the instrument is operated in negative mode.

In the other examples investigated, $Os_6(CO)_{18}$ showed somewhat reduced levels of aggregation, whereas Ru_6C-

(15) (a) Braunstein, P., Oro, L. A., Raithby, P. R., Eds. *Metal Clusters in Chemistry*; John Wiley & Sons: New York, 1999. (b) Dyson, P. J.; McIndoe, J. S. *Transition Metal Carbonyl Cluster Chemistry*; Gordon and Breach: Amsterdam, 2000.
(16) Butcher, C. P. G.; Dyson, P. J.; Johnson, B. F. G.; Khimyak, T.; McIndoe, J. S. *Chem.—Eur. J.* **2003**, *9*, 944.
(17) (a) Wang, X B.; Wang, L. S. *Phys. Rev. Lett.* **1999**, *83*, 3402. (b) Wang, L. S.; Wang, X. B. *J. Phys. Chem. A* **2000**, *104*, 1978.
(18) Butcher, C. P. G.; Johnson, B. F. G.; McIndoe, J. S.; Yang, X.; Wang, X. B.; Wang, L. S. *J. Chem. Phys.* **2002**, *116*, 6560.
(19) Critchley, G.; Dyson, P. J.; Johnson, B. F. G.; McIndoe, J. S.; O'Reilly, R. K.; Langridge-Smith, P. R. R. *Organometallics* **1999**, *18*, 4090.
(20) (a) Dale, M. J.; Dyson, P. J.; Johnson, B. F. G.; Martin, C. M.; Langridge-Smith, P. R. R.; Zenobi, R. *J. Chem. Soc., Chem. Commun.* **1995**, 1689. (b) Dale, M. J.; Dyson, P. J.; Johnson, B. F. G.; Langridge-Smith, P. R. R.; Yates, H. T. *J. Chem. Soc., Dalton Trans.* **1996**, 771.
(21) Dyson, P. J.; McGrady, J. E.; Reinhold, M.; Johnson, B. F. G.; McIndoe, J. S.; Langridge-Smith, P. R. R. *J. Cluster Sci.* **2000**, *11*, 391.
(22) Dollard, W. J.; Dyson, P. J.; Jackson, T.; Johnson, B. F. G.; McIndoe, J. S.; Langridge-Smith, P. R. R. *Inorg. Chem. Commun.* **1999**, *2*, 587.

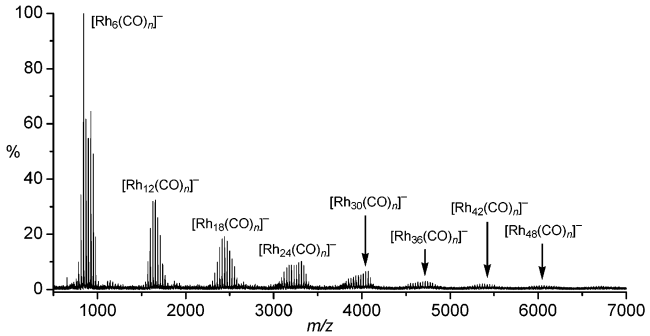

Figure 2. Negative ion LDI mass spectrum of $Rh_6(CO)_{16}$ **18**.

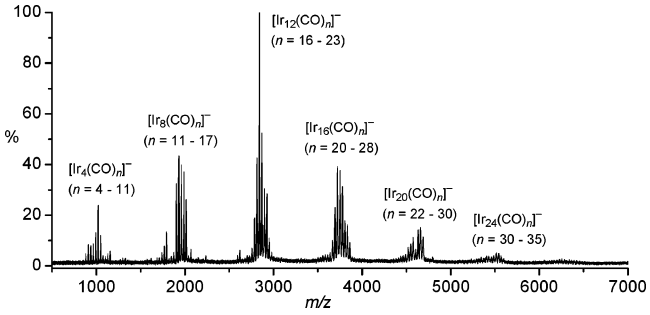

Figure 3. Negative ion LDI mass spectrum of $Ir_4(CO)_{12}$ **20** in the range 500−7000 *m*/*z*. See Supporting Information (Table SI.1) for full peak listings and assignments.

$(CO)_{17}$ showed much more, with the observation of $[(Ru_6C)_{30}(CO)_{\sim 85}]^+$ at over 20 000 *m*/*z* and evidence for higher aggregates still. Replacement of CO by arene ligands appeared to suppress the extent of the supraclustering process.

The negative ion LDI mass spectrum of $Ir_4(CO)_{12}$ **20** is shown in Figure 3. The spectrum is markedly different from those of the $[M_3(CO)_{12}]$ clusters, because supraclustering in units of four metal atoms is observed. The absence of the parent peak at ca. 1104.9 *m*/*z*, corresponding to the intact $[Ir_4(CO)_{12}]^-$ cluster species, is as expected on the basis of observations of similar cluster complexes.[19] The neutral parent $Ir_4(CO)_{12}$, according to the effective atomic number (EAN) rule, is an electron-precise cluster with 60 valence electrons (VE), and it is not expected to undergo electron capture without CO dissociation. Peak centroids for the tetranuclear cluster are observed at ca. 1076.6, 1049.6, 1021.8, 994.0, 965.9, 936.1, 910.0, and 880.1 *m*/*z* corresponding to successive losses of CO ligands (28 mass units apart) to generate the series $[Ir_4(CO)_n]^-$ ($n = 4-11$).

The next series of peaks at ca. 2016.6, 1988.1, 1960.2, 1931.6, 1901.6, 1871.5, and 1845.6 *m*/*z* corresponds to $[Ir_8(CO)_n]^-$ ($n = 11-17$) and is thought to occur by the coalescence of two unsaturated $[Ir_4(CO)_x]^{+/0/-}$ clusters. Two tetrahedral units probably combine to form a bicapped octahedron, which will probably rearrange to form a polytetrahedral structure. The highest nuclearity species for this peak envelope at ca. 2013.6 corresponds to $[Ir_8(CO)_{17}]^-$, 107 VE, which by polyhedral skeletal electron pair theory (PSEPT)[24] is consistent with the proposed geometric structure. The peaks in the range 2758−2953 *m*/*z* correspond to $[Ir_{12}(CO)_n]^-$ ($n = 16-23$). In this case, three tetrahedra have combined, and the valence electron count for $[Ir_{12}(CO)_{23}]^-$ is 155. This is four electrons short of the structure expected if another tetrahedral unit simply fused onto the bicapped octahedron $[Ir_8(CO)_{17}]^-$, suggesting that rearrangement to a more condensed polyhedral core has taken place. Scheme 1 gives an example of a coalescence process and includes two possible structures for the rearranged dodecanuclear core, a three-layer close-packed array and a polytetrahedral *nido*-icosahedron.

Three further series of peaks appear in the spectrum in the ranges 3637−3862, 4463−4689, and 5452−5593 *m*/*z*, corresponding to $[Ir_{16}(CO)_n]^-$ ($n = 20-28$), $[Ir_{20}(CO)_n]^-$ ($n = 22-30$), and $[Ir_{24}(CO)_n]^-$ ($n = 30-35$), respectively. The fact that the Ir/CO ratio drops to less than 1.5 for Ir_{24} indicates a high degree of decarbonylation from the starting material **20**, which has an Ir/CO ratio of 3. This observation is in keeping with the other homoleptic clusters reported previously and also suggests a high degree of polyhedral rearrangement.

Close inspection of the spectrum reveals that secondary processes have taken place. A series of low-intensity peaks in the range ca. 1685−1823 *m*/*z* correspond to $[Ir_7(CO)_n]^-$ ($n = 12-17$), and another series of peaks with low relative intensities in the range ca. 1073−1157 *m*/*z* correspond to $[Ir_5(CO)_n]^-$ ($n = 4-7$). An expansion of these ranges is illustrated in Figure 4.

This suggests that the process $[Ir_4(CO)_{12}]^{+/0/-} \rightarrow [Ir_3(CO)_x]^{+/0/-} + [Ir(CO)_y]^{+/0/-}$ occurs. These reactive fragments can subsequently react with the much more abundant tetranuclear species present, giving rise to the Ir_5 and Ir_7 series. Because of the high energies involved in the LDI process, the ejection of a metal fragment to decrease the internal energy of the cluster is plausible, though this process had only previously been observed for trinuclear clusters.[19,25] The fact that no Ir_6 species appear suggests that the process $Ir_4(CO)_{12} \rightarrow 2Ir_2(CO)_x$ is not important, probably because one more Ir−Ir bond (from 6 to 2) would effectively have to be broken than in the $Ir_4 \rightarrow Ir_3 + Ir$ case (from 6 to 3). The absence of $[Ir(CO)_x]^-$ and $[Ir_3(CO)_y]^-$ in the mass spectrum is attributed to their high reactivity. Two further higher-nuclearity series are present (i.e., $[Ir_{11}(CO)_n]^-$ ($n = 15-20$) and $[Ir_{15}(CO)_n]^-$ ($n = 20-25$) in the ranges 2534−2675 and 3416−3556 *m*/*z*), presumably generated from the reaction of the Ir_3 species with Ir_8 and Ir_{12} supraclusters, respectively.

The positive ion LDI mass spectrum of **20** is similar to the negative ion spectrum. In contrast, however, in the parent ion region, the intact molecular ion $[Ir_4(CO)_{12}]^+$ is observed. Also, the distribution of clusters is subtly different, with slightly less decarbonylation for a given metal nuclearity,

(23) For examples of very large clusters, see (a) Tran, N. T.; Kawano, M.; Powell, D. R.; Dahl, L. F. *J. Am. Chem. Soc*. **1998**, *120*, 10986. (b) Tran, T.; Dahl, L. F. *Angew. Chem., Int. Ed.* **2003**, *42*, 3533. (c) Tran, N. T.; Powell, D. R.; Dahl, L. F. *Angew. Chem., Int. Ed*. **2000**, *39*, 4121. (d) Amoroso, A. J.; Gade, L. H.; Johnson, B. F. G.; Lewis, J.; Raithby, P. R.; Wong, W. T. *Angew. Chem., Int. Ed. Engl.* **1991**, *30*, 107.

(24) Evans, D. G.; Mingos, D. M. P. *Organometallics* **1983**, *2*, 435.

(25) Dyson, P. J.; Hearley, A. K.; Johnson, B. F. G.; McIndoe, J. S.; Langridge-Smith, P. R. R. *Inorg. Chem. Commun.* **1999**, *2*, 591.

Scheme 1. Possible Coalescence/Rearrangement Pathway for the Aggregation of $Ir_4(CO)_n$ Units That Fits the LDI-MS Data

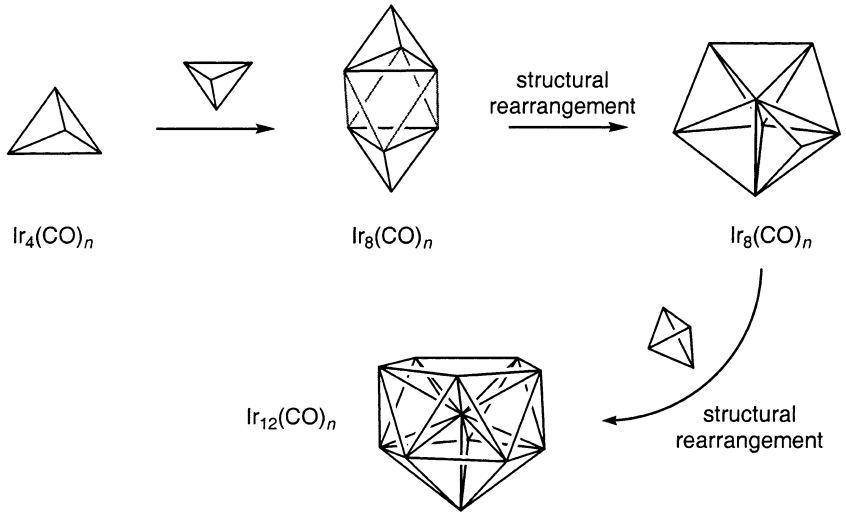

and less supraclustering takes place. Both of these features are consistent with the idea that the loss of an electron does not enforce decarbonylation, which contrasts with the negative ion species. Reduced decarbonylation should lead to lower reactivity and hence less supraclustering.

The LDI mass spectrum of the hexanuclear planar raft-type cluster $Os_6(CO)_{21}$ **21** is shown in Figure 5. In contrast to all of the other LDI spectra of neutral homoleptic clusters, **21** shows (practically) no supraclustering (very low intensity peaks corresponding to $[Os_{12}(CO)_n]^-$ aggregates are observed, suggesting the aggregation of octahedral species and not the open cluster). The spectrum consists essentially of two series of peaks, 1261−1371 *m*/*z* corresponding to $Os_5(CO)_n$ (n = 11−15) and 1479−1730 *m*/*z* corresponding to $Os_6(CO)_n$ (n = 12−21). The facile loss of one osmium atom may be attributed to the fact that the open raft structure of $Os_6(CO)_{21}$ has three osmium atoms bound to the cluster by just two bonds. It has already been established that trinuclear clusters (in which each metal has a connectivity of two) undergo extensive fragmentation of the metal core under LDI conditions. The lack of reactivity toward aggregation of the cluster units is also presumably a function of the open cluster framework. Usually, ablation of a cluster leads simply to loss of carbonyl ligands, the resulting coordinative unsaturation leads to high reactivity, and the formation of new metal−metal bonds which takes place during aggregation reduces the extent of unsaturation. However, upon losing CO ligands, $Os_6(CO)_{21}$ can reduce its degree of unsaturation by the formation of intramolecular metal−metal bonds (see Scheme 2).

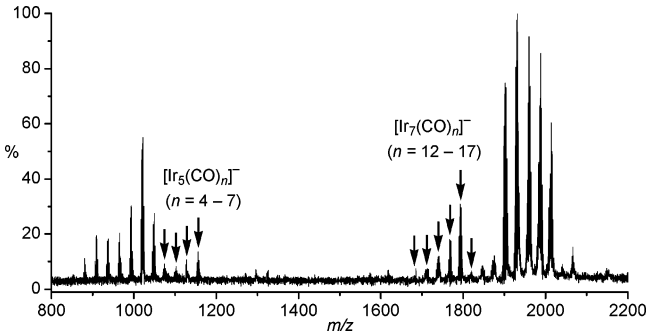

Figure 4. Negative ion LDI mass spectrum of $Ir_4(CO)_{12}$ **20** in the region 800−2200 *m*/*z*.

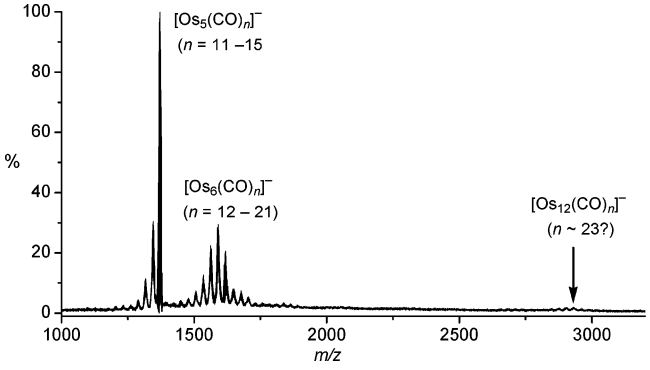

Figure 5. Negative ion LDI mass spectrum of $Os_6(CO)_{21}$ **21** in the region 1000−3200 *m*/*z*. See Supporting Information (Table SI.2) for full peak listings and assignments.

This "folding-up" process to more compact skeletal geometries means that, even after $Os_6(CO)_{21}$ loses three CO ligands, it is coordinatively saturated and hence unreactive toward aggregation. On the basis of such a hypothesis, one would expect that if $Os_6(CO)_{18}$ **19** itself was exposed to LDI conditions then ablation of the cluster should cause the loss of CO ligands without recourse to structural rearrangement, making it susceptible to supraclustering. $Os_6(CO)_{18}$ has been examined in a separate study and does indeed supracluster under LDI conditions, and fragmentation of the metal core is not observed.[25] Compensation for CO ligand loss by the formation of new metal−metal bonds is a process that has been inferred in studies of the fragmentation of open clusters using CID in conjunction with ESI.[16]

The pentanuclear square pyramidal cluster $Ru_5C(CO)_{15}$ **22** contains a carbide ligand that is essentially enclosed and unreactive. The LDI−MS of this cluster did not show any unexpected features, and the carbide does not seem to participate other than to confer stability to the cluster core and prevent fragmentation, a well-known effect for an interstitial carbon atom.[26] Aggregation extended out only as

Scheme 2. Rearrangement of the Open Raft Structure of $Os_6(CO)_{21}$ **21** via Intramolecular M−M Bond Formation

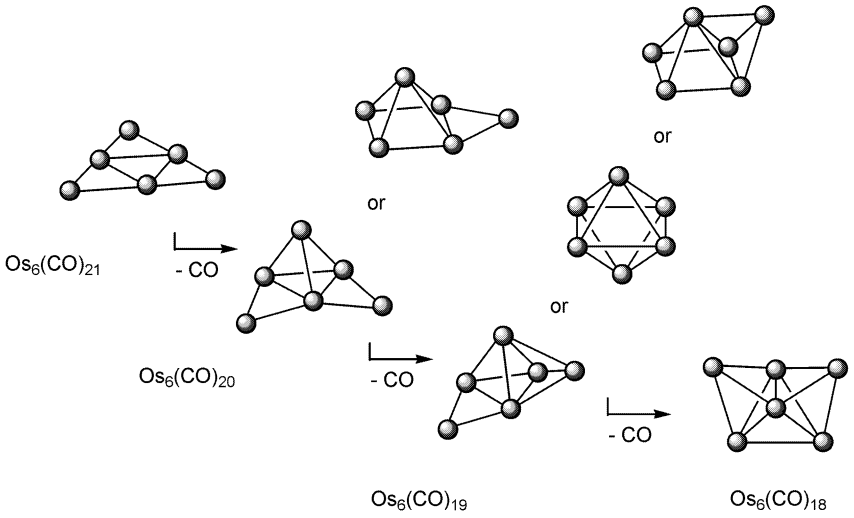

far as $[Ru_{25}C_5(CO)_{34}]^-$, somewhat more limited than that observed for the related octahedral cluster $Ru_6C(CO)_{17}$.

Heteronulear Homoleptic Clusters. The LDI mass spectrum of $Os_2Ru(CO)_{12}$ **23** is shown in Figure 6. The products observed are based on both homonuclear species, viz., $[Os_3]^-$ and $[Os_5]^-$, and heteronuclear species, viz., $[Os_2Ru_2]^-$, $[Os_2Ru_3]^-$, $[Os_4Ru]^-$, $[Os_4Ru_2]^-$, $[Os_5Ru]^-$, $[Os_4Ru_3]^-$, $[Os_5Ru_3]^-$, and $[Os_5Ru_4]^-$. There are no examples of homonuclear ruthenium cluster anions, and the ratio of ruthenium to osmium exceeds 1 only for $[Os_2Ru_3]^-$. No peaks corresponding to dinuclear species are observed in the spectrum.

The possible structures of the aggregation products can be predicted using the EAN rule or the PSEPT, depending upon the size of the metal core. Figure 7 illustrates the likely structures of the clusters predicted using these rules. It should be noted that the lifetime of these clusters is extremely short, on the order of microseconds, hence they are kinetic and not thermodynamic products, and therefore, they may not necessarily exhibit electronically saturated structures.

For each cluster unit, it is assumed that the highest mass peak for each cluster core is derived from a neutral species with one additional CO ligand because in the parent region $[Os_2Ru(CO)_{11}]^-$ is derived from **23**. The LDI-TOF mass spectra of $Os_3(CO)_{12}$ and $Ru_3(CO)_{12}$ have been reported previously,[19] and there are many similarities between the higher-mass species observed in all three spectra. The tetranuclear cluster units are based on $[Os_2Ru_2]^-$ and $[Os_3Ru]^-$ cores. The highest mass signal for the former is centered at 945 *m*/*z*, corresponding to $[Os_2Ru_2(CO)_{13}]^-$, a 59 cve species, 1 short of that expected for a tetrahedral core; the tridecacarbonyl cluster is the only one observed for the latter.

Four different combinations of pentanuclear cores are observed, and the highest mass signal of each corresponds to the 71 electron species $[Os_xRu_{5-x}(CO)_{15}]^-$ ($x = 5, 4, 3, 2$), which, taking into account the requirement for the loss of one CO ligand in order for the cluster to acquire the charge, leads to the prediction of trigonal bipyramidal skeleta. Hexanuclear species based on $[Os_4Ru_2(CO)_n]^-$ and $[Os_5Ru(CO)_n]^-$ structures are observed; both have a maximum of 17 CO ligands, corresponding to a bicapped tetrahedral core. The only heptanuclear clusters are based on the $[Os_4Ru_3(CO)_n]^-$ core, which, with a maximum of 20 CO ligands, means that a capped octahedral core is predicted. Peaks corresponding to octa- and enneanuclear clusters with low intensities are present, but the main species appear to be based on the $[Os_5Ru_3(CO)_n]^-$ and $[Os_5Ru_4(CO)_n]^-$ series. The low intensity of the signals, combined with overlapping peaks in the region, means that assignments are made with considerably less confidence than those for the lower-mass series, but are probably based on polytetrahedral geometries.

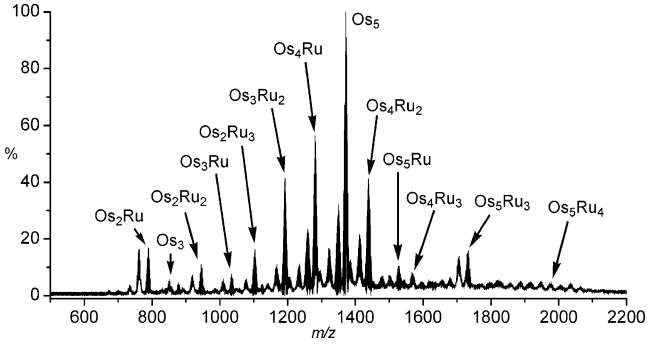

Figure 6. Negative ion LDI mass spectrum of $Os_2Ru(CO)_{12}$ **23** in the region 500−2200 *m*/*z*. See Supporting Information (Table SI.3) for full peak listings and assignments.

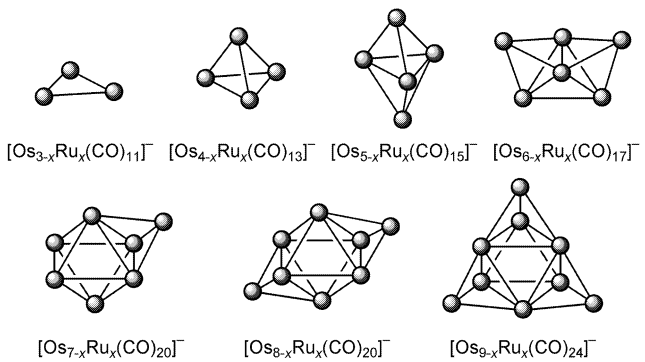

Figure 7. PSEPT-predicted cluster core structures for the species observed in the negative ion LDI mass spectrum of $Os_2Ru(CO)_{12}$ **23**.

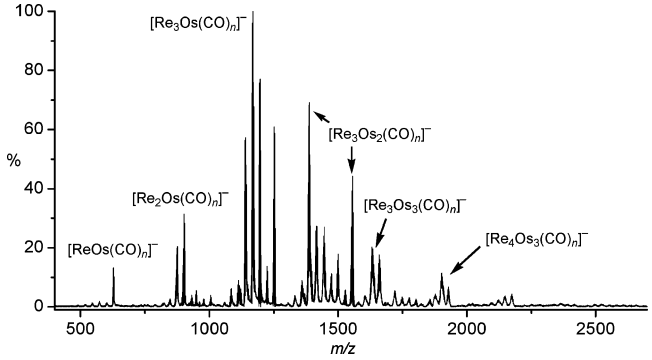

Figure 8. Negative ion LDI mass spectrum of $Re_2Os(CO)_{14}$ **25** in the region 400−2700 *m*/*z*. See Supporting Information (Table SI.4) for full peak listings and assignments.

The linear clusters $M_2Os(CO)_{14}$ (M = Mn **24** and Re **25**) have also been analyzed by LDI−MS. (An improved method for their synthesis was developed; see the Experimental Section.) The negative ion UV LDI mass spectrum of $Re_2Os(CO)_{14}$ **25** is shown in Figure 8.

The spectrum of **25** exhibits a peak at 929 *m*/*z* that corresponds to $[Re_2Os(CO)_{13}]^-$, along with additional peaks spaced ca. 28 *m*/*z* apart that correspond to the sequential loss of carbonyl ligands. Peaks at lower masses, in the region 572−628 *m*/*z*, correspond to heteronuclear bimetallic $[ReOs]^-$ species. The most intense peak in this series is the one centered at 628 *m*/*z* that corresponds to $[ReOs(CO)_9]^-$, which fulfills the 18 electron rule assuming that the charge is localized on the osmium. The presence of the binuclear species shows that metal−metal bond cleavage, in addition to ligand stripping, takes place during laser ablation, an important observation for the discussion of the higher mass peaks.

Ions corresponding to $[Re_3Os(CO)_n]^-$, $[Re_3Os_2(CO)_n]^-$, $[Re_3Os_3(CO)_n]^-$, and $[Re_4Os_3(CO)_n]^-$ are observed. It is reasonable to assume that the $[Re_3Os(CO)_n]^-$ and $[Re_3Os_2(CO)_n]^-$ clusters are formed from direct ion−molecule reactions as shown in, for example, eqs 1 and 2:

$$[Re(CO)_n]^- + Re_2Os(CO)_m \rightarrow [Re_3Os(CO)_{n+m}]^- \quad (n + m = 12-18) \quad (1)$$

$$[ReOs(CO)_x]^- + Re_2Os(CO)_y \rightarrow [Re_3Os_2(CO)_{x+y}]^- \quad (x + y = 14-22) \quad (2)$$

The higher-nuclearity clusters could be derived from either the aggregation of the mono-, di-, and trinuclear species produced during laser ablation or from the $[Re_3Os]^-$ and $[Re_3Os_2]^-$ products.

In the region 1086−1254 *m*/*z*, clusters based on the tetranuclear Re_3Os core are observed. The peak at 1254 *m*/*z* corresponds to the species $[Re_3Os(CO)_{18}]^-$, which would contain three metal−metal bonds. Possible structures for $[Re_3Os(CO)_n]^-$ (n = 15−18) are shown in Scheme 3 (those with osmium in a terminal position are not shown).

All of these structures obey the EAN rule, hence removal of one ligand from the most open structures, viz., $[Re_3Os(CO)_{18}]^-$, necessitates the formation of a 2c−2e metal−metal bond, leading to either spiked triangular or rectangular structures as shown in Scheme 3. Further CO loss gives rise to the formation of a butterfly structure, and two isomers are possible depending upon whether the Os atom is located in a hinge or wing-tip position. Loss of one additional carbonyl will give rise to a 60 VE tetrahedron, the most compact shape for a tetranuclear cluster. The peak centered at 1170 *m*/*z* corresponds to the 60 VE cluster $[Re_3Os(CO)_{15}]^-$, the most intense peak in the entire spectrum. As carbonyl ligands are removed from the tetrahedral core, peaks centered at 1142, 1114, and 1086 *m*/*z* are observed, which correspond to $[Re_3Os(CO)_{14}]^-$, $[Re_3Os(CO)_{13}]^-$, and $[Re_3Os(CO)_{12}]^-$, respectively.

Scheme 3. Possible Structures for $[Re_3Os(CO)_n]^-$ (n = 15−18)

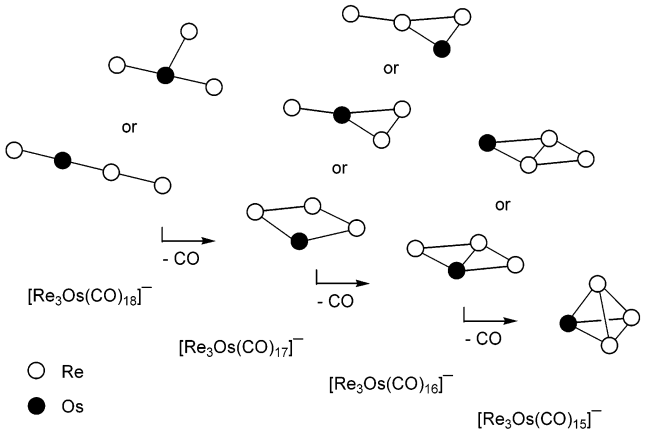

Pentanuclear clusters based on $[Re_3Os_2(CO)_n]^-$ (n = 14−22) are observed between 1332 and 1554 *m*/*z*. An increasing number of structures are possible, and they are illustrated in Scheme 4. (For simplicity, the majority of Re and Os atoms are not distinguished.) The highest mass peak in this region corresponds to the anion $[Re_3Os_2(CO)_{22}]^-$, and in the linear structure if all of the CO ligands were terminal, then the charge would presumably reside on the central Re atom.

From the data available, it is not possible to ascertain any other information about these species, and they will not be commented on further. The peak centered at 1416 *m*/*z* corresponds to the 72 VE species $[Re_3Os_2(CO)_{17}]^-$. An electron count of 72 corresponds to a trigonal bipyramid geometry that is the most compact arrangement for a pentanuclear cluster. Further CO loss from the trigonal bipyramid core is observed with the formation of $[Re_3Os_2(CO)_{16}]^-$, $[Re_3Os_2(CO)_{15}]^-$, and $[Re_3Os_2(CO)_{14}]^-$ at 1388, 1360, and 1332 *m*/*z*, respectively.

Hexanuclear clusters with Re_3Os_3 cores are observed in the range 1603−1659 *m*/*z*. The highest-mass species in the series corresponds to the 84 VE cluster $[Re_3Os_3(CO)_{19}]^-$. This electron count corresponds to a bicapped tetrahedron, the most compact arrangement for a hexanuclear cluster. The other two clusters in the series are therefore electronically unsaturated; it has been noted previously that, as the nuclearity of clusters observed in the LDI-TOF mass spectrometer increases, the degree of electronic saturation decreases.[19] The heptanuclear clusters observed between 1846

(26) Dyson, P. J. *Adv. Organomet. Chem.* **1999**, *43*, 43.

Scheme 4. Possible Structures for $[Re_3Os_2(CO)_n]^-$ ($n = 17-22$)

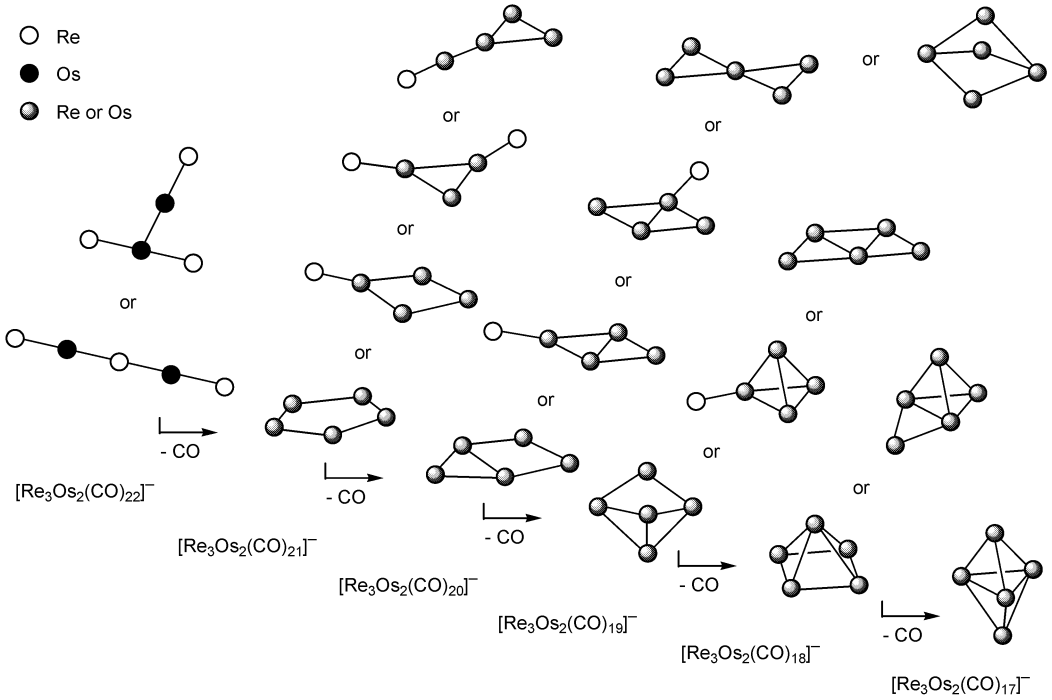

and 1930 *m*/*z* are based on Re_4Os_3 cores. Like the clusters in the previous species, the heptanuclear species are compact, presumably having a polytetrahedral core. With the exception of the electronically saturated cluster $[Re_4Os_3(CO)_{22}]^-$, the remainder are unsaturated. The LDI mass spectrum of $Re_2Ru(CO)_{14}$ is very similar to that of $Re_2Os(CO)_{14}$, and essentially all of the arguments stated already hold for both clusters.

The major process for trinuclear clusters, linear or triangular, is fragmentation of the metal core followed by aggregation of the resulting metal fragments. It is interesting to contrast the behavior of the linear (open) cluster with the raft, $Os_6(CO)_{21}$, which is also open and forms only very limited aggregates. Presumably, this difference is due to the fact that the raft cluster has only 50% more CO ligands but can compensate for the loss of three (rather than just one) through M−M bond formation.

Analysis by LDI-MS of mixtures of clusters composed of different metal types, dissolved in solution and deposited on the sample probe, did not result in the formation of heteronuclear clusters. Instead, spectra showing the characteristic peaks of the individual clusters were obtained, presumably because the different clusters form homogeneous microcrystals on the sample probe.

Nonhomoleptic Clusters. The negative ion LDI-TOF mass spectra of $Ru_3(CO)_{12-n}(PPh_3)_n$ ($n = 1$ **26**, 2 **27**, and 3 **28**) have been reported previously.[25] The PPh_3 ligands do not remain coordinated to the cluster, which results in spectra characteristic of the homoleptic precursor $Ru_3(CO)_{12}$ **13**. In addition to all of the PPh_3 ligands being stripped from the cluster, one or more CO ligands are always lost for the clusters in the molecular ion region, and as the number of phosphine ligands in the parent cluster increases, the extent of fragmentation peaks and gas-phase aggregation products also increases. Clearly, LDI-MS does not represent a good method for determining the molecular weight of such species and cannot be used as an analytical method.

Replacing one or more carbonyl ligands by acetonitrile on a cluster represents an excellent way of increasing its reactivity because the acetonitrile ligand is more labile. In fact, high-nuclearity osmium clusters are generally prepared by vacuum pyrolysis, but triosmium dodecacarbonyl is not very reactive, and $[Os_3(CO)_{12-n}(MeCN)_n]$ (where $n = 1$ and 2 **29**) and $[H_2Os_3(CO)_{10}]$ **30** tend to be used as starting materials, giving a far greater range of products, generally with higher nuclearities.[27] The negative ion LDI mass spectrum of $Os_3(CO)_{10}(MeCN)_2$ **29** is shown in Figure 9. The notable aspect of this spectrum is the difficulty in assigning the low-mass peaks corresponding to Os_3 and Os_4 cores; sensible combinations of Os, CO, and MeCN do not correspond exactly to any of the peaks in this region, and this observation is indicative of post-source decay (PSD). Post-source decay has been observed in the LDI mass spectra of transition metal clusters before,[21] but the phenomenon of ligand loss during transit through the flight tube is usually only a problem for high-mass clusters with very many CO ligands. The fact that we observe the process here at low mass suggests that we are observing facile loss of the weakly bound acetonitrile ligands. None of the higher-mass clusters contain acetonitrile ligands, and all provide excellent matches between calculated and experimental isotope patterns.

The series of peaks observed in the region 1300−1400 *m*/*z* has been assigned to the pentanuclear cluster anions formed by the partial decarbonylation of $[Os_5(CO)_{16}]$. The highest-intensity peak is at ca. 1372 *m*/*z*, corresponding to $[Os_5(CO)_{15}]^-$. Further CO loss results in the peaks centered

(27) Lewis, J.; Raithby, P. R. *J. Organomet. Chem.* **1995**, *500*, 227.

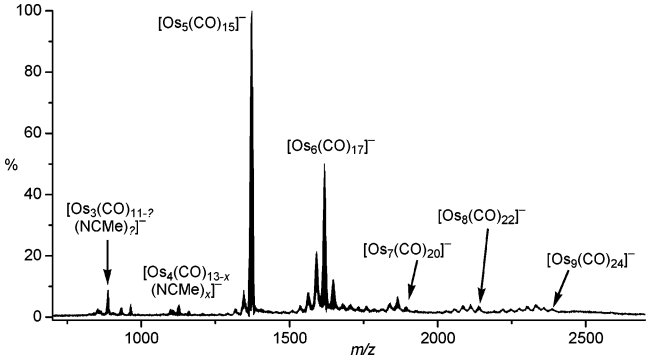

Figure 9. Negative ion LDI mass spectrum of $Os_3(CO)_{10}(MeCN)_2$ **29** in the region 700−2700 *m*/*z*. See Supporting Information (Table SI.5) for full peak listings and assignments.

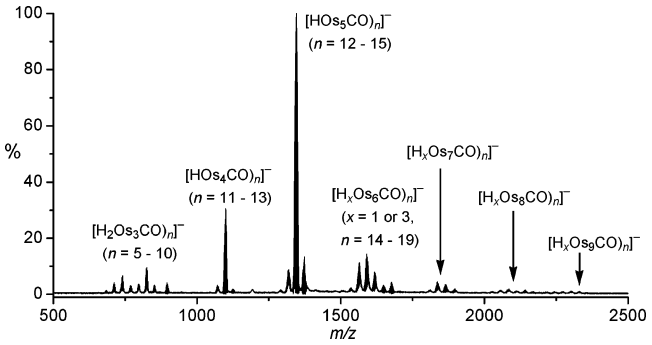

Figure 10. Negative ion LDI mass spectrum of $H_2Os_3(CO)_{10}$ **30** in the region 500−2500 *m*/*z*. See Supporting Information (Table SI.6) for full peak listings and assignments.

at 1344 and 1316 *m*/*z*, which correspond to $[Os_5(CO)_{14}]^-$ and $[Os_5(CO)_{13}]^-$, respectively. The next series of peaks in the range 1648−1534 *m*/*z* corresponds to the cluster anions $[Os_6(CO)_n]^-$ (n = 14−18). The comparatively high abundance of the Os_5 and Os_6 species may be indicative of a primary cluster buildup mechanism that involves the condensation of two Os_3 units to make Os_6 species; excess internal energy may be dispersed by elimination of a mononuclear fragment to generate the Os_5 clusters.

A series of high-intensity peaks are observed in the range 1750−1891 *m*/*z*, which may be assigned as $[Os_7(CO)_n]^-$ (n = 15−20). The expected parent would be the $Os_7(CO)_{21}$, a known capped octahedron cluster. At the highest masses, 2054−2160 *m*/*z*, a number of peaks are clearly visible and may be readily assigned as $[Os_8(CO)_n]^-$ (n = 19−22). The final series of peaks in the range 2385−2272 *m*/*z* has been assigned as $[Os_9(CO)_n]^-$ (n = 20−24). The relatively high abundance of Os_9 species may support the proposal that a significant contribution to the buildup process for this cluster is in Os_3 units. Compared to the LDI mass spectrum of $Os_3(CO)_{12}$, more extensive clustering is observed for $Os_3(CO)_{10}(MeCN)_2$. The highest-nuclearity product formed in both the pyrolysis and LDI-MS of $Os_3(CO)_{12}$ is $Os_8(CO)_{23}$.

A representative negative ion mass spectrum of $H_2Os_3(CO)_{10}$ **30** is shown in Figure 10. The first point of interest is the parent peak ca. 853 *m*/*z*, corresponding to $[H_2Os_3(CO)_{10}]^-$. The title compound is electronically unsaturated with only 46 VE, with a possible metal−metal double bond[28] or, alternatively, a four-center (Os_2H_2) four-electron bond.[29] It is therefore not surprising that this cluster is able to accommodate another electron without the dissociation of a carbonyl ligand. Other peak centroids in this series at ca. 825, 798, 742, 712, and 684 *m*/*z* correspond to CO dissociation. The hydride ligands associated with this cluster do not dissociate until the cluster has lost five carbonyl ligands, possibly because of rearrangement and symmetry requirements.

The next series of peaks at ca. 1127, 1099, and 1071 *m*/*z* corresponds to $[HOs_4(CO)_{13}]^-$, $[HOs_4(CO)_{12}]^-$, and $[HOs_4(CO)_{11}]^-$, respectively. This series is thought to occur from the fragmentation of the parent cluster, followed by an [ion]−[parent neutral] reaction (i.e., $[Os(CO)_x]^-$ (x = 1−4) and $[H_2Os_3(CO)_{10}]$), followed by ligand dissociation and rearrangement to produce the tetrahedral series.

$$[Os(CO)_x]^- + H_2Os_3(CO)_{10} \rightarrow [HOs_4(CO)_y]^- \quad (y = 13-11)$$

The next series of peaks at ca. 1374, 1345, 1317, and 1289 *m*/*z* corresponds to $[HOs_5(CO)_{15}]^-$, $[HOs_5(CO)_{14}]^-$, $[HOs_5(CO)_{13}]^-$, and $[HOs_5(CO)_{12}]^-$, respectively. This series, similar to $[HOs_4(CO)_y]^-$, is thought to occur by the reaction between a $[H_xOs_2(CO)_y]^-$ and a neutral parent molecule, undergoing a similar process to produce the trigonal bipyramid series.

The series in the range 1677−1535 *m*/*z*, corresponding to $[H_xOs_6(CO)_y]^-$ where y = 19−14 and x = 3 or 1, is very interesting and provides evidence for a number of possible reactions. The peak centroids at ca. 1590.7 and 1564.8 *m*/*z* are attributed to $[HOs_6(CO)_{16}]^-$ and $[H_3Os_6(CO)_{15}]^-$, respectively. Both isotope patterns match well, hence a high degree of confidence is founded in the assignments; structures are likely to be polytetrahedral (bicapped tetrahedral), by electron counting. The highest-mass peak in this envelope corresponds to $[H_xOs_6(CO)_{19}]^-$, which by electron counting rules must represent an open cluster, one of very few examples observed in the aggregate clusters. It is quite clear that the reactions occurring are indeed rather complex, and it would be unwise to postulate possible reaction mechanisms at this stage. The next three series of peaks in the range 2302−1810 *m*/*z* correspond to nuclearities of 7 to 9. These peaks are thought to occur by secondary reactions (i.e., the capping of Os_5 or Os_6 species by either $[H_xOs(CO)_y]$, $[H_xOs_2(CO)_y]$, or $[H_xOs_3(CO)_y]$ units).

The appearance of pentanuclear Os_5 species as the base peaks in all spectra of the osmium clusters studied (see Figures 5, 6, 9, and 10) is worth further comment. In the cases of the spectra resulting from **29** and **30**, the particularly high abundance of the Os_5 species is probably due to a combination of synthetic pathways: reaction between two Os_3 species followed by elimination of a mononuclear fragment and reactions between Os_3 and Os_2 or 2 × Os species can all contribute to the formation of Os_5 species.

(28) (a) Wade, K. *J. Chem. Soc., Chem. Commun.* **1971**, 792. (b) Wade, K. *Adv. Inorg. Chem. Radiochem.* **1976**, *18*, 1. (c) Wade, K. *Inorg. Nucl. Chem. Lett.* **1972**, *8*, 559. (d) Wade, K. *Inorg. Nucl. Chem. Lett.* **1972**, *8*, 563. (e) Wade, K. *Inorg. Nucl. Chem. Lett.* **1972**, *8*, 823. (f) Wade, K. *Nature (London), Phys. Sci.* **1972**, *240*, 71.

(29) Thanks to a referee for pointing out this alternative view of the bonding.

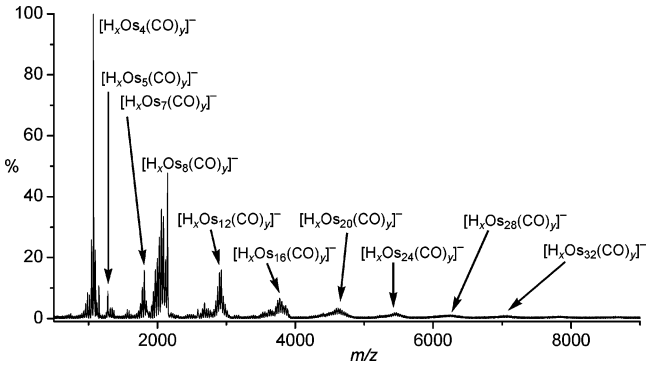

Figure 11. Negative ion LDI mass spectrum of $H_4Os_4(CO)_{12}$ **32** in the region 500−9000 *m*/*z*. See Supporting Information (Table SI.7) for full peak listings and assignments.

In the case of **21**, the high abundance of Os_5 is almost certainly due to the fact that three of the Os atoms are bonded to the cluster with just two Os−Os bonds each and removal of one is relatively easy. The high abundance of Os_5 from **23** is the least explicable case, especially in light of the fact that Os_4 species are of very low intensity, but its observation does suggest particular stability of the pentanuclear framework.

The negative ion LDI−TOF mass spectra of the tetrahedral hydrido clusters $H_4Ru_4(CO)_{12}$ **31**, $H_4Os_4(CO)_{12}$ **32**, $H_2RuOs_3(CO)_{13}$ **33**, $H_2FeRu_3(CO)_{13}$ **34**, and $H_2FeOs_3(CO)_{13}$ **35** have been recorded, and that of $H_4Os_4(CO)_{12}$ **32** is shown in Figure 11 as a representative example. Peaks are listed with their corresponding (tentative) assignments in the Supporting Information. In the heteronuclear clusters, **33**−**35**, no homonuclear cluster anions are observed, and the ratio of the two metals in each precursor remains unchanged in the aggregation products. This feature suggests that the integrities of their metal cores remain intact, which is characteristic of homoleptic tetrahedral clusters.

There are special difficulties associated with the interpretation of spectra containing many labile hydride ligands. Elimination of a single H^+ can provide a detectable anion, $[M-H]^-$, but during the processes of fragmentation and aggregation, loss of H_2 can readily occur. Estimation of the number of H ligands in the higher aggregates is problematic; in addition to overlap of isotopomer envelopes for aggregates of the form $[H_xM_y(CO)_z-nH_2]^-$, signal intensity diminishes (reducing the signal-to-noise ratio), and resolution decreases with higher *m*/*z*. These factors conspire to make a confident assignment of the number of hydride ligands present extremely difficult, and as such, the tables listing peak assignments do not attempt a definitive assignation. The triangular hydride clusters $[HM(CO)_4]_3$ (M = Mn **36**, Re **37**) were also shown to supracluster,[30] and assignments in this case could be made with greater confidence because of the lower nuclearities of the aggregates formed and the fact that the isotopomer envelopes of the products were simpler (Mn is monoisotopic, and Re has two isotopes).

The sulfur-containing cluster $Ru_3(\mu_3\text{-}S)(CO)_{10}$ **38** is a derivative of $Ru_3(CO)_{12}$ **13** in which two CO ligands have been replaced by a face-capping S atom.[31] The core of the cluster can be viewed as pseudotetrahedral, and therefore, it was of interest to determine whether the binding influence of the heteroatom would be sufficient to hold together the cluster units under LDI conditions, as in the tetrametal clusters. Indeed, supraclustering in Ru_3S units is the dominant process, but in addition, significant amounts of other clusters also form, indicating that some fragmentation of the parent also takes place. On the basis of the products formed, the fragmentation process appears to comprise $Ru_3S(CO)_x \rightarrow Ru_2S(CO)_x + Ru(CO)_z$. Free sulfur, $RuS(CO)_x$, $Ru_3(CO)_x$, or $Ru_2(CO)_x$ fragments do not appear to be produced (Scheme 5).

Scheme 5. Proposed Fragmentation Products Based on the Observed and Absent Aggregation Products Identified in the LDI-MS of $Ru_3(\mu_3\text{-}S)(CO)_{10}$ **38**[a]

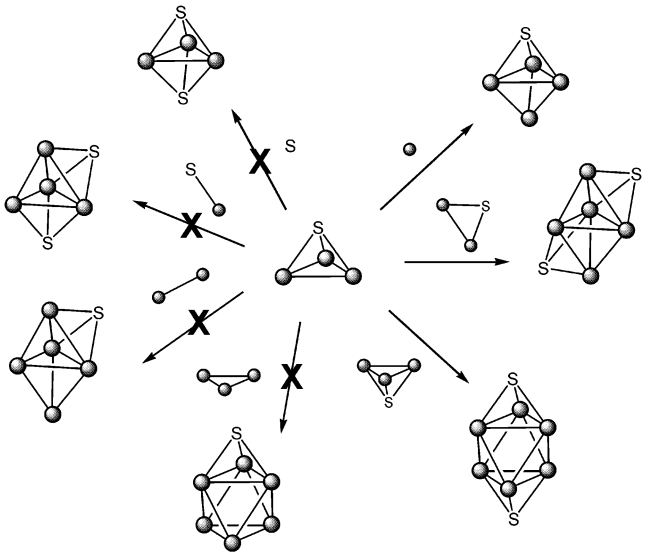

[a] See supporting information (Table SI.8) for full peak listings and assignments.

The first peak envelopes centered at 559−587 *m*/*z* correspond to the parent ion region $[Ru_3S(CO)_n]^-$ (n = 8−9), with the expected loss of CO to accommodate the negative charge. The next series of peaks between 717 and 745 *m*/*z* corresponds to $[Ru_4S(CO)_n]^-$ (n = 10−11) and represents the parent cluster combining with $Ru(CO)_x$ fragments. The next series at 877−933 *m*/*z* is formed by the remaining fragment, $Ru_2S(CO)_x$, combining with the parent cluster to form $[Ru_5S_2(CO)_n]^-$ (n = 11−13). Two unsaturated parents aggregate together to form the strong series from 1007 to 1118 *m*/*z*, corresponding to $[Ru_6S_2(CO)_n]^-$ (n = 12−16). The remaining peaks all conform to this pattern. Peaks at 1164−1176 *m*/*z* correspond to $[Ru_7S_2(CO)_n]^-$ (n = 14−18), at 1325−1437 *m*/*z* to $[Ru_8S_3(CO)_n]^-$ (n = 15−19), the strongest series at 1453−1623 *m*/*z* to $[Ru_9S_3(CO)_n]^-$ (n = 16−22), and a weak series at 1676−1785 *m*/*z* to $[Ru_{10}S_3(CO)_n]^-$ (n = 20−24). A weak peak envelope centered at 2071 *m*/*z* probably corresponds to $[Ru_{12}S_4(CO)_{26}]^-$.

Speculating on the structure of these clusters is difficult because of the coordinative flexibility of the sulfur ligand, which can be face-capping or interstitial. However, the Ru_3S/

(30) Dyson, P. J.; Hearley, A. K.; Johnson, B. F. G.; McIndoe, J. S.; Langridge-Smith, P. R. R. *J. Chem. Soc., Dalton Trans.* **2000**, 2521.

(31) Adams, R. D.; Babin, J. E.; Tasi, M. *Inorg. Chem.* **1986**, *25*, 4514.

CO ratio drops from 1:10 in the parent cluster to a little over 1:2 in $[Ru_{12}S_4(CO)_{26}]^-$, representing significant decarbonylation, and hence, the core of the higher-nuclearity clusters rearranges considerably to form compact structures rather than a chain of loosely linked cluster units (not too dissimilar to the $Ir_4(CO)_{12}$ example shown in Scheme 1). The possibility of structures in which the aggregates are composed of dative bonds between the sulfur lone pair on one fragment with the ruthenium or another atom cannot be ruled out. In fact, such a reaction may well take place and facilitate the aggregation process; however, because the ratio of Ru_3S/CO is very low, the actual clusters detected contain considerably more compact cores than those generated by such a mechanism. The sulfur bridges in the platinum dimer $Pt_2(\mu\text{-}S)_2(PPh_3)_4$ have been shown to react with other metal ions to form multinuclear species that have been characterized by ESI-MS and other methods.[32]

The clusters $Ru_5C(CO)_{15}$ **22** and $Ru_5PtC(CO)_{16}$ **39** contain a carbide ligand, and in both, the carbide is essentially enclosed and unreactive. The LDI-MS of these clusters do not show any unexpected features, and the carbide does not seem to participate other than to confer stability to the cluster cores and prevent fragmentation. $H_3NiOs_3(CO)_9(\eta\text{-}C_5H_5)$ **40** shows very limited supraclustering behavior, and $Ni_3Os_3(CO)_9(\eta\text{-}C_5H_5)_3$ **41** shows none whatsoever; presumably, the strongly bound cyclopentadienyl ligand resists removal and suppresses gas-phase reactivity by blocking reactive sites and preventing M−M bond formation.

The series $Br[Os(CO)_4]_nBr$ (n = 1 **42**, 2 **43**, 3 **44**) was analyzed by LDI-MS. The peaks appear to be characteristic of those observed for other metal carbonyl complexes, but on close inspection, it transpires that none of the signals may be reasonably assigned (i.e., no match of a combination of the elements Os, Br, C, and O satisfied m/z and isotope pattern criteria), and all of the peaks correspond to PSD peaks. The only difference between these compounds and the others studied is the presence of the Br ligand, and it is tempting to attribute the PSD process to the elimination of a Br-containing neutral fragment, most likely Br_2. This explanation partially accounts for the large deviation from the calculated positions of likely fragments/aggregates because although PSD processes are observed for the binary metal carbonyls, the loss of CO in the flight tube has a fairly minor effect on the position of the signal.[21] Thus, considerable caution must be applied to the LDI-MS analysis of metal carbonyl clusters with halide ligands.

Conclusions

Combining the observations made for the behavior of the various carbonyl clusters under LDI allows the following generalizations to be made:

(i) Clusters that include metal atoms with two or less metal−metal bonds are prone to fragmentation, and the nuclearity of the observed species often bears no relationship to the nuclearity of the target cluster.

(ii) Clusters that contain metal atoms with three or more metal−metal bonds tend to aggregate in multiples of the original nuclearity.

(iii) Open clusters may not aggregate at all because they can compensate for decarbonylation by polyhedral rearrangement to a more compact metal core.

(iv) Partial decarbonylation is a characteristic feature of all spectra, and the extent of decarbonylation is more pronounced for the higher aggregates.

(v) Substantial M−M bond formation and metal core rearrangement likely occur upon aggregation.

The neutral clusters that underwent aggregation in multiples of the original nuclearity all showed very extensive decarbonylation as well as aggregation, a feature of the LDI spectra depicted in Figure 12.

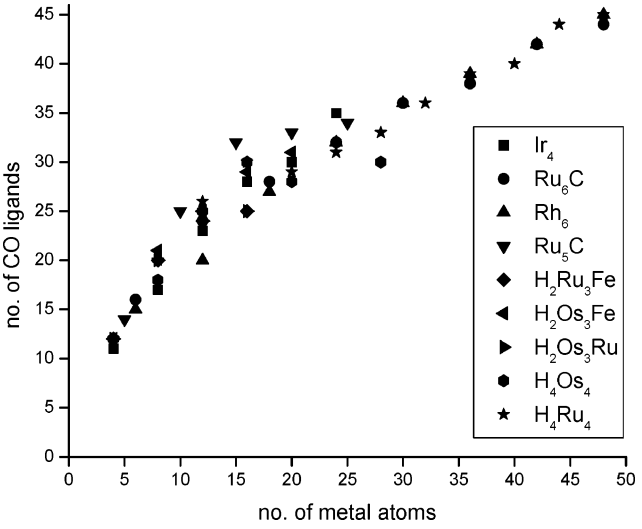

Figure 12. Plot of ($x \times n$) vs z for the aggregate ions $[(M_x)_n(CO)_z]^-$ observed for a variety of neutral tetra, penta, and hexanuclear (x = 4, 5, 6) carbonyl clusters.

If the clusters were aggregating by a simple linking process, then the ratio of CO/M should be more or less maintained as the clusters build up in nuclearity. However, the fact that the ratio drops from approximately 3 for the original clusters to less than 1 for the higher aggregates is good evidence for rearrangement of the metal atoms such that they constitute a near-spherical core surrounded by a shell of surface CO ligands.

In terms of using LDI-TOF MS as a method for determining the molecular weight of clusters, we have shown that, although it is possible for the majority of clusters examined, a great deal of other information is required that really limits the utility of the technique. Anionic clusters are nonetheless relatively straightforward to identify; however, the data must also be combined with electron counting rules because multiply charged species are reduced to monoanions. Hence, the technique is only as good as the electron counting rules, and an increasing number of clusters do not obey these rules.[33]

(32) (a) Fong, S. W. A.; Vittal, J. J.; Henderson, W.; Hor, T. S. A.; Oliver, A. G.; Rickard, C. E. F. *Chem. Commun*. **2001**, 421. (b) Fong, S. W. A.; Yap, W. T.; Vittal, J. J.; Henderson, W.; Hor, T. S. A.; Oliver, A. G.; Rickard, C. E. F. *J. Chem. Soc., Dalton Trans.* **2001**, 1986.

(33) Adams, R. D.; Captain, B.; Fu, W.; Hall, M. B.; Manson, J.; Smith, M. D.; Webster, C. E. *J. Am. Chem. Soc.* **2004**, *126*, 5253.

Experimental Section

Compounds $[Ru_3Co(CO)_{13}]^-$,[34] $[Ru_3Ir(CO)_{13}]^-$,[35] $[H_3Os_4(CO)_{12}]^-$,[36] $[HRu_6(CO)_{18}]^-$,[37] $[Ru_5CoC(CO)_{16}]^-$, and $[Ru_5IrC(CO)_{16}]^-$,[38] $[Fe_6C(CO)_{16}]^{2-}$,[39] $[Ru_6C(CO)_{16}]^{2-}$,[40] $[Re_8C(CO)_{24}]^{2-}$,[41] $[HRu_{10}C(CO)_{24}]^-$,[42] $[Os_{10}C(CO)_{24}]^{2-}$,[43] $Os_2Ru(CO)_{12}$,[44] $H_2RuOs_3(CO)_{13}$, $H_2FeRu_3(CO)_{13}$, and $H_2FeOs_3(CO)_{13}$,[45] $Ru_5PtC(CO)_{16}$,[46] $H_3NiOs_3(CO)_9(\eta\text{-}C_5H_5)$, and $Ni_3Os_3(CO)_9(\eta\text{-}C_5H_5)_3$,[47] $Os_6(CO)_{18}$,[48] $Os_6(CO)_{21}$,[49] $H_2Os_3(CO)_{10}$,[50] and $Os_3(CO)_{10}(NCMe)_2$ [51] were prepared according to literature methods. $Ir_4(CO)_{12}$ and $Rh_6(CO)_{16}$ were purchased from Strem. Samples were dissolved in dichloromethane and deposited onto the sample probe. The solvent was allowed to evaporate, leaving a thin layer of the pure sample. Several layers were added in this manner and analyzed using a Micromass TOFSpec2E. An improved method for the preparation of $Re_2Os(CO)_{14}$ will be described; essentially, the same preparation was used for the synthesis of $Re_2Ru(CO)_{14}$.

Synthesis of $Re_2Os(CO)_{14}$. $Os_3(CO)_{12}$ (0.100 g, 0.110 mmol) was reduced with sodium metal in liquid ammonia under argon. After 3 h of intermittent stirring, the dianionic $Na_2[Os(CO)_4]$ formed as a white solid.[52] The excess liquid ammonia was allowed to evaporate while stirring under a stream of argon. $Re(CO)_5Br$ (0.27 g, 0.67 mmol) in tetrahydrofuran (20 mL) was added with stirring at −78 °C and allowed to warm to room temperature overnight. $Re_2Os(CO)_{14}$ was isolated by fractional crystallization from a minimal amount of warm acetone and further sublimed at 90 °C under dynamic vacuum to produce pale yellow crystals (0.23 g, 0.24 mmol, 70% yield).

Acknowledgment. We thank Tony Jackson for assistance in collecting some of the LDI data.

Supporting Information Available: Data for compounds $Ir_4(CO)_{12}$ **20**, $Os_6(CO)_{21}$ **21**, $Ru_5C(CO)_{15}$ **22**, $Os_2Ru(CO)_{12}$ **23**, $Re_2Os(CO)_{14}$ **25**, $Os_3(CO)_{10}(MeCN)_2$ **29**, $H_2Os_3(CO)_{10}$ **30**, $H_4Ru_4(CO)_{12}$ **31**, $H_4Os_4(CO)_{12}$ **32**, $H_2RuOs_3(CO)_{13}$ **33**, $H_2FeRu_3(CO)_{13}$ **34**, $H_2FeOs_3(CO)_{13}$ **35**, $Ru_3(CO)_{10}(\mu_3\text{-}S)$ **38**, $Ru_5PtC(CO)_{16}$ **39**, $Os_3Ni_3(CO)_9Cp_3$ **40**, and $H_3Os_3NiCp(CO)_9$ **41**. The material is available free of charge via the Internet at http://pubs.acs.org.

IC049458I

(34) Fox, J. R.; Gladfelter, W. L.; Geoffroy, G. L. *Inorg. Chem.* **1980**, *19*, 2574.
(35) Johnson, B. F. G.; Quadrelli, E.; Ferrand, V.; Bott, A. W. *J. Chem. Soc., Dalton Trans.* **2001**, 1063.
(36) Johnson, B. F. G.; Lewis, J.; Raithby, P. R.; Sheldrick, G. M.; Wong, K.; McPartlin, M.; William, J. H. *J. Chem. Soc., Dalton Trans.* **1978**, 673.
(37) Jackson, P. F.; Johnson, B. F. G.; Lewis, J.; McPartlin, M.; William, J. H. *J. Chem. Soc., Chem. Commun.* **1979**, 735.
(38) Dyson, P. J.; Hearley, A. K.; Johnson, B. F. G.; Khimyak, T.; McIndoe, J. S.; Langridge-Smith, P. R. R. *Organometallics* **2001**, *20*, 3970.
(39) Hill, E. W.; Bradley, J. S.; Cassidy, J.; Whitmire, K. H. *Inorg. Synth.* **1989**, *27*, 183.
(40) Hayward, C. M. T.; Shapley, J. R. *Inorg. Chem.* **1982**, *21*, 3816.
(41) Ciani, G.; D'Alfonso, G.; Freni, M.; Romiti, P.; Sironi, A. *J. Chem. Soc., Chem. Commun.* **1982**, 705.
(42) Bailey, P. J.; Johnson, B. F. G.; Lewis, J.; McPartlin, M.; Powell, H. R. *J. Organomet. Chem.* **1989**, *377*, C17.
(43) Jackson, P. F.; Johnson, B. F. G.; Lewis, J.; William, J. H.; McPartlin, M. *J. Chem. Soc., Dalton Trans.* **1982**, 2099.
(44) Johnson, B. F. G.; Johnston, R. D.; Lewis, J.; Williams, I. J.; Kilty, R. A. *J. Chem. Soc., Chem. Commun.* **1968**, 861.
(45) Geoffroy, G. L.; Fox, J. R.; Burkhardt, E.; Foley, H. C.; Harley, A. D.; Rosen, R. *Inorg. Synth.* **1982**, *21*, 57.
(46) Adams, R. D.; Wu, W. *Organometallics* **1993**, *12*, 1238.
(47) Bergounhou, C.; Bonnet, J. J.; Lavigne, G.; Papageorgiou, F. *Inorg. Synth.* **1989**, *26*, 360.
(48) Nichols, J. N.; Vargas, M. D.; Adams, R. D.; Natarajan, K. *Inorg. Synth.* **1989**, *26*, 295.
(49) Gouldsmit, R. J.; Jeffrey, J. G.; Johnson, B. F. G.; Lewis, J.; McQueen, R. C. S.; Whitmire, A. J.; Lui, J. C. *J. Chem. Soc., Chem. Commun.* **1986**, 24.
(50) Kaesz, H. D.; Glavee, G. N.; Angelici, R. J. *Inorg. Synth.* **1990**, *28*, 238.
(51) Nichols, J. N.; Vargas, M. D. *Inorg. Synth.* **1990**, *28*, 289.
(52) Shore, S. G. *Organometallics* **1985**, *4*, 1483.